ROYAL SOCIETY OF CHEMISTRY

Journal Name

ARTICLE

Magnetic domain wall tweezers: a new tool for mechanobiology studies on individual target cells

M. Monticelli,[a] D. V. Conca,[a] E. Albisetti,[a] A. Torti,[a] P. P. Sharma,[a] G. Kidiyoor,[c] S. Barozzi,[c] D. Parazzoli,[c] P. Ciarletta,[d] M. Lupi,[e] D. Petti,[a] and R. Bertacco[a,b]

In vitro tests are of fundamental importance for investigating cell mechanisms in response to mechanical stimuli or the impact of the genotype on the cell mechanical properties. In particular, the application of controlled forces to activate specific bio-pathways and investigate their effects, mimicking the role of the cellular environment, is becoming a prominent approach in the emerging field of mechanobiology. Here we present an on-chip device based on magnetic domain wall manipulators, which allows for the application of finely controlled and localized forces on target living cells. In particular, we demonstrate the application of a magnetic force in the order of hundreds pN on the membrane of HeLa cells cultured on-chip, via manipulation of 1 μm superparamagnetic beads. Such mechanical stimulus produces a sizable local indentation of the cellular membrane of about 2 μm. Upon evaluation of the beads position within the magnetic field originated by the domain wall, the force applied during the experiments is accurately quantified via micromagnetic simulations. The obtained value is in good agreement with that calculated applying an elastic model to the cellular membrane.

Introduction

Nowadays, there is a growing need of versatile and miniaturized platforms for in-vitro fundamental biological and medical analysis. For example, drug screening[1,2] and gene therapy[3,4] are now principally based on in-vitro studies of cell cultures. Moreover, the ability of probing cellular dynamics and/or activating mechano-sensitive bio-pathways[5,6,7] allows to deeply investigate different mechano-transduction mechanisms, whose comprehension can be crucial for the diagnosis and treatment of many diseases[8,9]. Various studies are actually investigating how the application of controlled forces can affect the cellular response, highlighting specific mechanisms[10,11] such as differentiation[12], migration[13] and specific genes expression[14,15], in pathological and physiological conditions. In this field, named mechanobiology, different technologies were developed. A relevant example is provided by micromechanical stretching devices, e.g. microfluidic or microelectromechanical systems (MEMS)[16,17,18], whose typical feature size matches the micrometrical dimension of the mammalian cell. Another strategy is

using functional materials[19,20], such as PDMS[21] or gels[22], properly micro- and nanostructured to provide in vivo-like stimuli, mimicking those arising from the extracellular matrix. However, in most cases, cells are exposed to spatially homogenous, constant and pre-defined mechanical stimuli, preventing the study of localized mechanisms at sub-cellular level. A different approach is offered by patch-clamp[23] and atomic force microscopy (AFM)[24] based technologies, which exploit micrometric and nanometric tips to exert controlled forces. Both allow for the application of a localized mechanical stimulation, but patch-clamps are invasive, as they may easily damage cells and biomolecules, while AFM systems can not be easily integrated with high resolution microscopes for fluorescence based biological analysis. Moreover, these techniques do not allow to easily implement more than one experiment at a time.

In this context, micromanipulation techniques[25] based on the controlled and localized motion of micro and nanoparticles at the cellular and subcellular scale, are becoming a fundamental tool for testing the mechanical properties of cell sub compartments:, nucleus, cytoplasmic membrane and cytoskeleton. Furthermore, they are also extensively used for handling small biomolecules[26], e.g. in drug-delivery experiments. Among these micromanipulation techniques optical tweezers represent a well established technology. The first demonstration of trapping and manipulation of microparticles, viruses and bacteria via optical tweezers was provided by Ashkin and coworkers in 1986[27,28]. Although this technology presents good versatility and spatial resolution, some

a. Department of Physics, Politecnico di Milano, Milan, Italy.
b. IFN-CNR, c/o Politecnico di Milano, Milan, Italy.
c. Fondazione Istituto FIRC di Oncologia Molecolare (IFOM), Milan, Italy.
d. MOX, Department of Mathematics, Politecnico di Milano, Milan, Italy.
e. Department of Oncology, IRCCS – Istituto di Ricerche Farmacologiche "Mario Negri", Milan, Italy

drawbacks can be identified. First of all, the damage to the biological entities due to the laser-induced heating[29,30,31] and, secondly, the inherent complexity and cost of the optical setup. In the past years, alternative methods have been developed to overcome these limitations. Electrophoresis[32,33] and dielectrophoresis[34] based techniques are widely used, but they are strictly dependent on particle polarizability and medium conductivity. Furthermore, they utilize electrical forces that may adversely affect cell physiology due to current-induced heating and/or direct electric field interaction. In the same way, acoustic-based tweezers[35] induce unintentional heating due to power density requirements. In this context, magnetic manipulators[36,37,38,39] are very appealing because (i) they are suitable to operate in any biological environment, and (ii) they are non-invasive for cells and biomolecules, as the local energy dissipation is negligible if low frequency magnetic fields are applied. On-chip patterned ferromagnetic elements, whose magnetization creates a confined stray field, have been employed to attract and manipulate particles with a micrometric resolution[40]. In this context, some of the authors proposed a magnetic handling technology, called "Domain wall Tweezers" (DWTs)[41,42,43,44]. It is based on the displacement of magnetic domain walls (DWs) in ferromagnetic conduits, allowing for the manipulation of magnetic micro and nanoparticles with resolution down to 100 nm[41]. The on-chip trapping and manipulation of yeast cells in suspension, properly decorated with magnetic beads, has been also demonstrated[45].

In this paper, we present a platform based on magnetic DW tweezers, suitable for mechanobiology studies. DWs propagating in ferromagnetic rings are exploited to finely manipulate superparamagnetic beads in a cellular environment so as to push them against the cellular membrane of HeLa cells cultured on-chip, thus exerting highly localized and controllable forces. The local deformation of the HeLa cells membrane and the exact position of the beads with respect to the conduit is observed via confocal microscopy. Then, the mechanical stimulus applied to the membrane is quantified, by calculating the magnetic force acting on the beads due to the stray field generated by the DW in the magnetic ring. Forces in the order of hundreds pN are exerted, producing cell indentations of about 2 μm, which are fully coherent with an elastic model of the HeLa cell membrane.

Our platform represents a versatile and non-invasive on-chip technology for mechanobiology studies on single cells, fully compatible with real time optical monitoring of the cell activity upon quantitative and localized mechanical stimulation.

Experimental methods

Experimental setup

A sketch of the experimental setup and the device working principle is reported in Figure 1a. Superparamagnetic beads are trapped and manipulated over ring-shaped ferromagnetic conduits in order to make them interact with cells cultured on-chip, exerting a magnetic force (F_m) to the cell membrane when an external magnetic field (H_e) is applied.

To monitor the particles manipulation during the experiments and imaging the effect of the mechanical stimuli on cells, a Leica TCS SP5 confocal laser scanning is used, based on a upright DM6000CFS microscope and equipped with HCX Apo L20x/1.0 NA W water immersion objective.

At the beginning of the experiments, the chip on which cells are cultured is gently washed in 2 ml of PBS to remove the cellular medium sediments on the surface, which could negatively affect the particles manipulation. Then, the chip is placed on a Petri dish in 1 ml of PBS, located in a microscope chamber with controlled temperature (37 °C) and wet atmosphere.

The external magnetic field needed to manipulate the DWs is applied using a couple of Neodymium Iron Boron ($Nd_2Fe_{14}B$) permanent magnets underneath the microscope stage. The field direction is set by a stepper motor which allows to finely control the magnets rotation, thus producing a uniform magnetic field mainly parallel the chip surface, with a maximum absolute value of 500 Oe. This field addresses simultaneously all the magnetic conduits.

The confocal microscopy images are elaborated by means of *ImageJ* software to analyze the cellular profiles, merge fluorescence images and obtain 3D cellular reconstructions from *z*-series images.

Device fabrication

The magnetic rings are made of Permalloy ($Ni_{80}Fe_{20}$). They are 150 nm thick, 2 μm wide and with radius of 10 μm. Reversed image optical lithography with AZ5214E resist and Karl Süss Mask Aligner MA6/BA8 is performed on Si substrate (1.5x1.5 cm^2) in order to pattern ring-shaped structure. Then, ion beam etching (Kaufman KDC 160 Ion Source, Kaufman & Robinson) is used in order to etch 150 nm of Si in the rings, thus obtaining planar samples after $Ni_{80}Fe_{20}$ deposition. E-beam evaporation (Evatec BAK 640 evaporator) and the subsequent lift-off allow to finally obtain 150 nm thick $Ni_{80}Fe_{20}$ rings. The magnetic conduits are then uniformly covered by a capping layer of Si_3N_4 (50 nm thick) and SiO_2 (50 nm thick), in order to ensure biocompatibility and prevent them from damages due to contact with the cell culture medium. Si_3N_4 films are grown by reactive RF magnetron sputtering (3" TORUS UHV Source (Kurt J Lesker)), while SiO_2 is grown by RF magnetron sputtering in pure Ar pressure (AJA ATC Orion 8 Sputtering System).

Cell culture and transfection

HeLa cells are grown in Eagle's minimum essential medium (MEM; Gibco-BRL), supplemented with non-essential amino acids, 10% (vol/vol) fetal bovine serum (not activated), 2 mM glutamine, 25mM HEPES and 100 μg/ml streptomycin in a humidified incubator (5% CO_2, 37°C). 36 hours before the experiment, cells are transfected with Lifeact-GFP[46] (F-actin marker for visualization of cytoplasm) using lipofectamine 2000 (Invitrogen). The day before the experiment, the micro-fabricated chips are placed in 6-well

dishes, cleaned with ethanol once, washed in PBS three times and then allowed to dry in the hood. Cells are plated onto the chip in order to achieve a cell confluence of approximately 50% during the experiment.

An optical image showing the chip with the transfected cells cultured on top is reported in Figure 1b.

coefficient τ= 0.01 and null magneto-crystalline anisotropy. A $25 \times 25 \times 20$ nm^3 unit cell has been used for simulating the micromagnetic configuration of the rings. Despite the exchange length of Permalloy is 5.2 nm, this represents a reasonable compromise ensuring reduced computational times. We have checked that using cubic unit cells with side of 5 nm does not
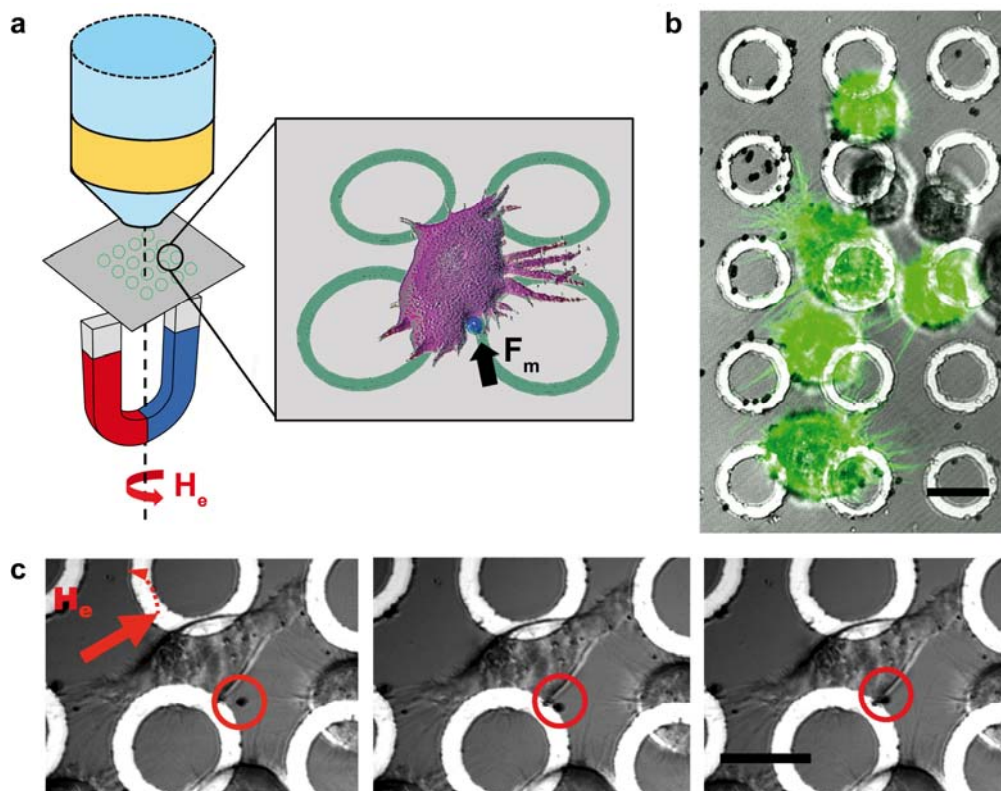
Figure 1: **a** Sketch of the experimental setup showing the chip with ring-shaped ferromagnetic nanostructures, the optical microscope to monitor the particles manipulation and the magnet for the application of a rotating external field (H_e). On the right, a zoom on the chip surface illustrates the device working principle: a superparamagnetic bead (blue) bound to a magnetic DW in the conduit exerts a magnetic force (F_m) on the cell membrane of a HeLa cell cultured on the chip surface. **b** Optical image showing the chip with the magnetic nanostructures and HeLa cells transfected with Lifeact-GFP (green fluorescence), after dispensation of 1 μm superparamagnetic beads (MyOne-Dynabeads). **c** Frames from a video showing the attraction and manipulation of 1 μm particle to the cellular membrane of a target HeLa cell when a rotating H_e= 300 Oe is applied. Scale bars: 20 μm

Magnetic Beads

Commercial MyOne®-dynabeads superparamagnetic particles functionalized with COOH are used (Invitrogen, 1 μm diameter, magnetization of saturation M_s= 35·10^3 A/m and magnetic susceptibility in the linear range χ_0= 1.46). They are diluted in phosphate buffer solution (PBS), to reach a final concentration of 1 μg/ml. The values of M_s and χ_0 are measured by Vibrating Sample Magnetometer (VSM) (see Supplementary Information).

Micromagnetic simulations and magnetic force calculations

Simulations to quantify the force applied by the domain wall magnetic tweezers are performed with OOMMF (Object Oriented Micro Magnetic Framework)[47]. The micromagnetic configuration of the rings and related magnetic stray field are calculated using the following parameters for Ni$_{80}$Fe$_{20}$: saturation magnetization M_s= 680·10^3 A/m, exchange stiffness A= 1.3·10^{-11} J/m, damping

introduce major modifications in the simulated stray field.

The magnetic force is calculated from the stray field produced by the DW in the conduit, according to the following equation[48]:

$$\mathbf{F_m} = \frac{\mu_0}{2} \int_V \left[\nabla(\mathbf{M} \cdot \mathbf{H}) - H^2 \nabla(M/H) \right] dV \tag{1}$$

where $\mathbf{M}$ is the magnetization of the superparamagnetic bead, and $\mathbf{H}$ the total field ($H= H_d+H_e$), calculated with OOMMF, sum of the stray field generated by the ferromagnetic conduit (H_d) and the external magnetic field (H_e). The integration is performed numerically over the whole bead volume (V).

To improve the reliability of the force estimate we used the Langevin expression for the magnetic susceptibility, so as the local magnetization within the bead is given by:

$$M(H) = M_s \cdot \left(\coth\left(\frac{3\chi_0 \cdot H}{M_s} \right) - \frac{M_s}{3\chi_0 \cdot H} \right) \tag{2}$$

where M_S is the saturation magnetization and χ_0 is the linear magnetic susceptibility coefficient describing the linear dependence between M and H for small values of H.

Varying the beads concentration in solution, it is possible to promote the formation of bead clusters to increase the intensity of the applied mechanical stimuli. In order to estimate the magnetic force in such condition, a physical model including the dipolar interaction between beads is developed. As a matter of fact, the magnetization of each bead is affected by H_e, H_d and also by the magnetic stray field from the other particles in the cluster. In this way, the total field seen by each particle can be written as follows:

$$\mathbf{H_i} = \mathbf{H_e} + \mathbf{H_d} + \sum_{j \neq i} \frac{1}{4\pi} \left(\frac{3 r_{ij} (\mathbf{m_j} \cdot \mathbf{r_{ij}})}{r_{ij}^5} - \frac{\mathbf{m_j}}{r_{ij}^3} \right) \qquad (3)$$

where m_j is the magnetic moment of the j-th particle in the cluster and r_{ij} is the distance between the geometrical centres of beads i and j. The dipolar field is considered uniform all over the i-bead volume and, due to the fact that each $m_i(H_i)$ depends on the other beads magnetization (m_j), an iterative method to calculate the equilibrium magnetic configuration of the cluster has been developed. The H_i field and the magnetic moment of each particle are thus evaluated in a self-consistent way. Finally, the total force is calculated integrating Equation 1 over the whole cluster, with M and H given by Equations 2 and 3, respectively.

Results and discussion

Manipulation of magnetic beads in a cell culture environment

In Figure 1c, frames from a video (see SMovie1.avi in the Supporting Information) showing the working principle of our platform are reported. The DWs nucleated in magnetic rings allow for trapping and manipulating 1 µm bead so as to the cellular membrane of single HeLa cells cultured on chip, applying a rotating external magnetic field (H_e) of 300 Oe. The trapping is clearly visible looking at panels i and ii of Figure 1c, while the subsequent manipulation towards the cell membrane can be appreciated comparing panels ii and iii. As discussed in previous works[41,45,49], two opposite Néel DWs are nucleated in the ring, thus producing a magnetic stray field (H_d) whose gradient allows for the attraction and manipulation of particles in suspension. The magnetic configuration of a portion of ring has been simulated with OOMMF and it is shown in Figure 2a, for H_e= 300 Oe applied along the x-direction. The arrows represent the orientation of M in the magnetic conduit, showing that the DW magnetization is locally perpendicular to the ring in the region of the DW. The associated magnetic charges produce a confined stray field H_d which traps superparamagnetic beads in suspension. This fact can be clearly seen in Figure 2b where the simulated magnetic energy (U_m= $-\mu_0(m \cdot H)$) of 1 µm bead is shown as a function of the position in the x,y plane. Here, the particle is placed at a distance of 100 nm from the magnetic structure top surface, corresponding to the capping layer thickness. The potential well minimum is located above the DW, slightly displaced to the outer edge of the conduit[26].

Noteworthy, by rotating H_e in the chip plane, the Néel DW is moved along the ring in a continuous way, thus allowing the manipulation of the particles attracted above the nanostructures.

The maximum bead velocity achievable in a fluid is of the order of tens µm/s to ensure a synchronous motion of the bead and DW. In these conditions, the particle momentum is quite low ($\approx 10^{-20}$ kg m s^{-1}) and the force applied when a free bead hits the membrane is negligible. Even assuming an elastic scattering from the cell membrane (see video SMovie2.avi in the Supporting Information) in a typical interaction time of 0.1 s, the average force does not exceed 1 aN. This value is much lower than typical forces applied in mechanobiology studies, in the pN-nN range. As explained in the following, such values can be obtained exploiting the in-plane attractive force exerted by the domain wall on magnetic beads, continuously pushed against the cell membrane.

Simulations of Magnetic Forces exerted on cells

In order to use this DWTs technology for producing controlled mechanical stimuli, a quantification of the force that can be exerted on target cells is required. The mechanical force is essentially given by the magnetic force F_m on the beads, calculated according to Equation 1, as the latter is much higher than the other contributions acting on the magnetic bead: viscous friction, gravity, buoyancy and Brownian motion. The viscous friction on particles in a fluid is described by the Stokes equation (see Supplementary Information for details). For a typical manipulation velocity v= 10 µm/s, it is equal to 85 fN and can be neglected if compared to F_m, which is in the order of hundreds pN[41,49]. Even gravity and buoyancy forces are much less intense ($\approx$ 10 fN) than F_m. Finally, as discussed in ref. [26], the Brownian motion plays a negligible role when beads are trapped by DWTs because the thermal energy ($k_B T$= 4.14·10^{-21} J) is much lower than the magnetic one ($U_m \approx 10^{-16}$ J, see Figure 2b).

Figure 2c and 2d displays the simulated magnetic force maps on the x-y plane, for the radial (F_r, Figure 2c) and tangential (F_t, Figure 2d) components with respect to the magnetic ring, when H_e = 300 Oe is applied. The distance between the bottom of the bead and the top of the magnetic ring is set to 100 nm, in order to take into account the capping layer thickness.

The maximum values of the radial and tangential magnetic forces are, respectively, F_{rMAX} = 625 pN and F_{tMAX} = 215 pN. F_{rMAX} is higher than F_{tMAX} but the radial component is less confined than the tangential one, due to the peculiar micromagnetic configuration of the DW. The out-of-plane component of the force is even larger, up to 1 nN, but it is not shown because in the present paper we report on the manipulation of beads at the chip surface, so as to exert mainly in-plane forces to cells cultured on the chip. Crucial for applications, in ref. [49] some of the authors demonstrated that the magnetic force can be tuned varying the intensity of H_e, which affects the beads magnetization and consequently F_m (see the first term in Equation 1).
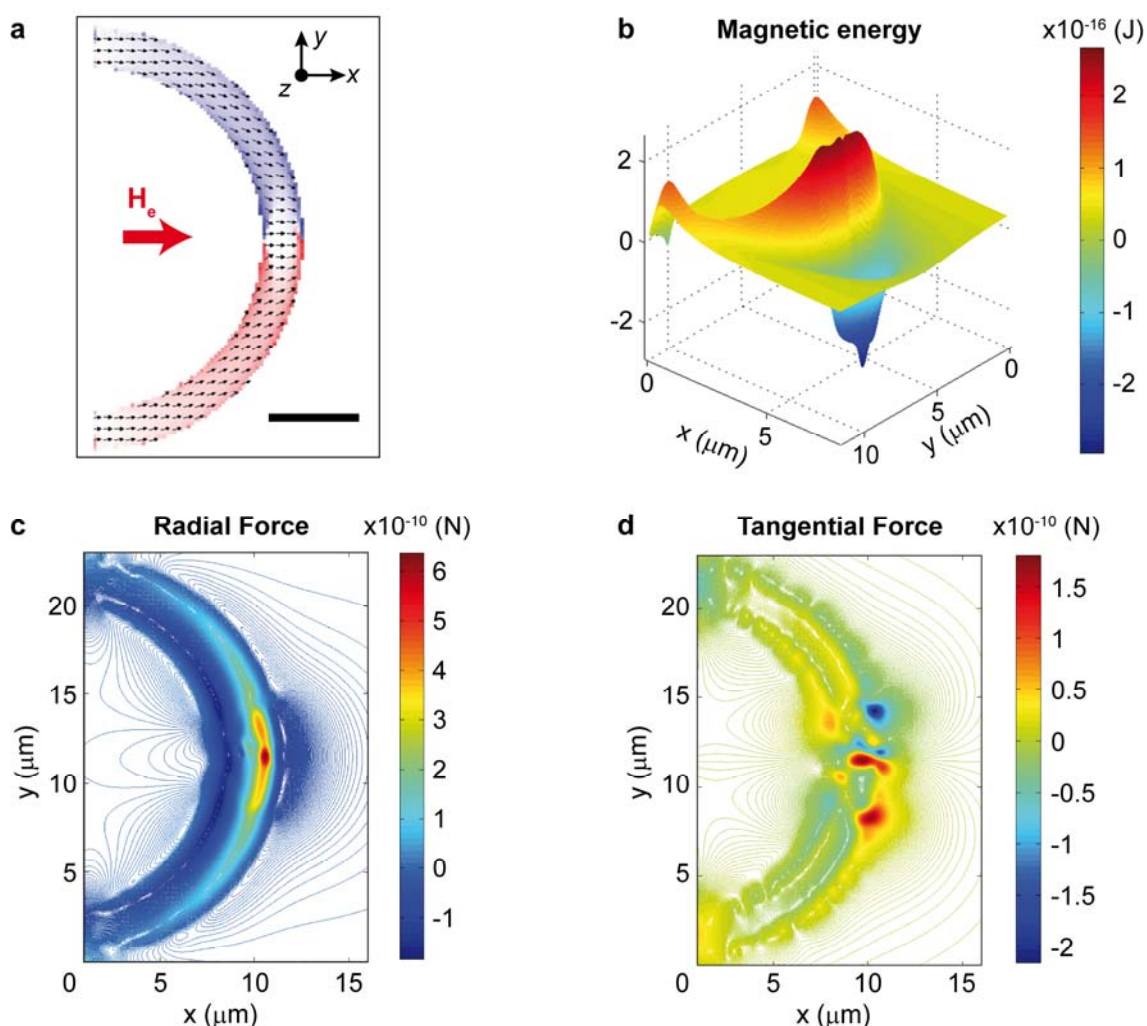
Figure 2: **a** Micromagnetic configuration (simulated with OOMMF) of a portion of the nanometric ring, where a transverse DW is nucleated by applying an external magnetic field (H_e) of 300 Oe directed along the x-axis. The arrows represent the local magnetization direction, while the red-white-blue scale refers to the y-component of the magnetization. Scale bar: 5 μm. **b** Magnetic energy well of a superparamagnetic bead (1 μm diameter, χ_0= 1.46, M_s= 35*10^3 A/m) attracted by the DW 100 nm above the ring shaped nano-conduit, when an external magnetic field of 300 Oe is applied. **c** Contour plot of the simulated radial component of the magnetic force in the *x-y* plane, exerted on a 1 μm magnetic bead with the bottom surface 100 nm above the nanostructure. **d** Same as in c for the force tangent to the ring.

Our platform thus provides an efficient method for applying localized and tuneable magnetic forces to the cell, whose intensity can be quantitatively evaluated and correlated to the observation of confocal microscopy. In fact, from the force maps reported in Figure 2c and 2d, F_m can be precisely calculated once the position of a bead with respect to the DW in the conduit is known.

Mechanical deformation of target cells membrane

In order to demonstrate the effectiveness of our technology, in this paper DWTs are used to produce a mechanical deformation on target HeLa cells membrane. Cells are cultured on microfabricated chips with the magnetic rings, as described in the methods. Then, beads are dispensed on the chip and, upon capture by a DW, manipulated to bring them in contact with the cell membrane (see

Figure 1c). Here, due to the opposite zeta-potential of the HeLa membrane (negative)[50] and beads (positive), an electrostatic interaction occurs. Indeed, some particles tend to bind to the membrane. When the DW is displaced bound particles initially apply a tensile strain to the cell membrane, until they detach when the attraction of the moving DW overcomes the electrostatic force. In this framework, the best configuration for applying sizable and durable forces is that corresponding to a compressive strain, or inwards force with respect to the cell, which can be achieved by pushing the beads against the membrane. This can be achieved by slightly displacing the DW towards the inner part of the cell, if the conduit crosses the cell contour line, or simply by exploiting the attraction from a DW in a conduit which is within the cell contour line. The second case is reported in Figure 3.
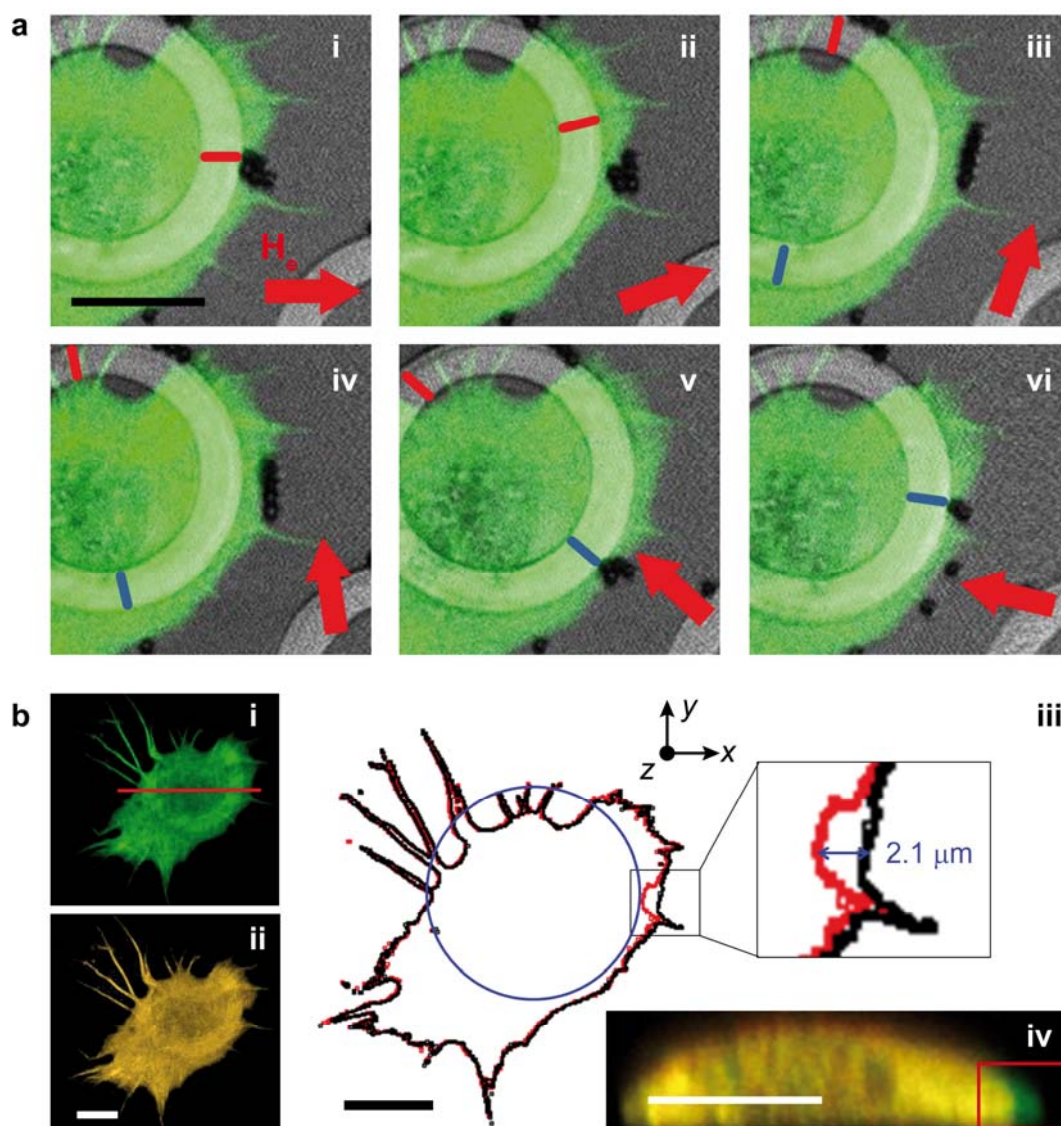
Figure 3: **a** Frames from a video showing the manipulation of a cluster of 5 superparamagnetic beads (MyOne Dynabeads, 1 μm) in contact to the cellular membrane of a green fluorescent HeLa cell (marked with Lifeact-GFP) when a rotating external field (H_e) of 300 Oe is applied. The DWs (red and blue lines) displaced along the magnetic ring by H_e, exert an attractive force on the beads, producing a local deformation of the cellular membrane. **b** Confocal image of the HeLa cell basal membrane before (i-green) and during (ii-orange) the local mechanical deformation. The data are acquired in about 60 s, after the application of the mechanical stimulus. Overlapped cellular profiles before (black) and during (red) the local membrane deformation are shown in panel b(iii). A reconstruction of a HeLa cell slice in the plane perpendicular to the chip surface corresponding to the red line in panel b(i) is reported in panel b(iv), before (orange) and during (green) the mechanical deformation. Scale bars: 10 μm

In Figure 3a(i-vi), some frames from a video show a cluster of magnetic beads in contact with a green fluorescent HeLa membrane, manipulated by DWTs. When rotating the in-plane external field (H_e= 300 Oe), the passage of the two opposite DWs (red and blue lines in Figure 3) provokes the attraction of the particles towards the ring edge, producing a local membrane deformation (Figure 3a(i)). As previously discussed, the beads stay attached to the cell membrane when the DW is displaced away. The magnetic force is released and the cell membrane recovers its initial equilibrium configuration (Figure 3a(ii)). When the DW is far away from the cluster, the particles are aligned along the external field direction (see Figure 3a(iii-iv)), but they are still bound to the cell membrane due to the electrostatic interaction. Instead, when the

DW approaches again the particles, they aggregate in a more compact configuration due to the localized attraction of the DW, (see Figure 3a(v)). The competition between electrostatic and magnetic forces is clearly seen comparing frames 3a(v) and 3a(vi). In this case, due to a quasi-static displacement of the DW, three particles follows the DW along the cell contour, whereas two of them remain attached to the membrane at the position previously occupied by the DW.

Deformed Cell Profile Analysis

In order to quantify and properly study the deformation produced by DWTs, a 3D profile analysis of the HeLa cell is carried-out. The

confocal microscope allows 3D imaging of cells with a lateral resolution lower than 500 nm and a vertical resolution of about 1 μm.

Such analysis is illustrated In Figure 3b and it is relative to the same cell shown in Figure 3a. The case in which no mechanical stimuli are applied to the membrane (see Figure 3b(i) green) is compared with the cell with a membrane invagination produced by magnetic beads (see Figure 3b(ii) where the actual green colour arising from fluorescence has been converted in orange to facilitate the comparison). Figures 3b(i-ii) report the cell basal membrane, acquired before and during the application of the force. This particular plane is selected because it identifies the position along z where the cluster of beads (trapped by the DW on the chip surface) is located.

Thanks to the high fluorescence signal intensity and to the low auto-fluorescence background, the cellular profiles are easily extracted from the fluorescence images and overlapped, as shown in Figure 3b(iii). In this way, a quantification of the membrane deformation is performed, leading to a maximum indentation of 2.1±0.5 μm in the selected cell plane. The error in the evaluation of the indentation depth is mainly due to the microscope resolution associated to some uncertainty during the profiles elaboration.

This result is confirmed by the cell sections displayed in Figure 3b(iv), obtained cutting it with a x-z plane whose projection is marked with red line in Figure 3b(i), before (green) and during (orange) the mechanical stimulation. A sizable membrane deformation is produced also along z-axis, in agreement with the micrometric size of the beads employed.

Note that, the reported data are relative to the equilibrium deformation of the cell membrane under the application of a constant mechanical load.
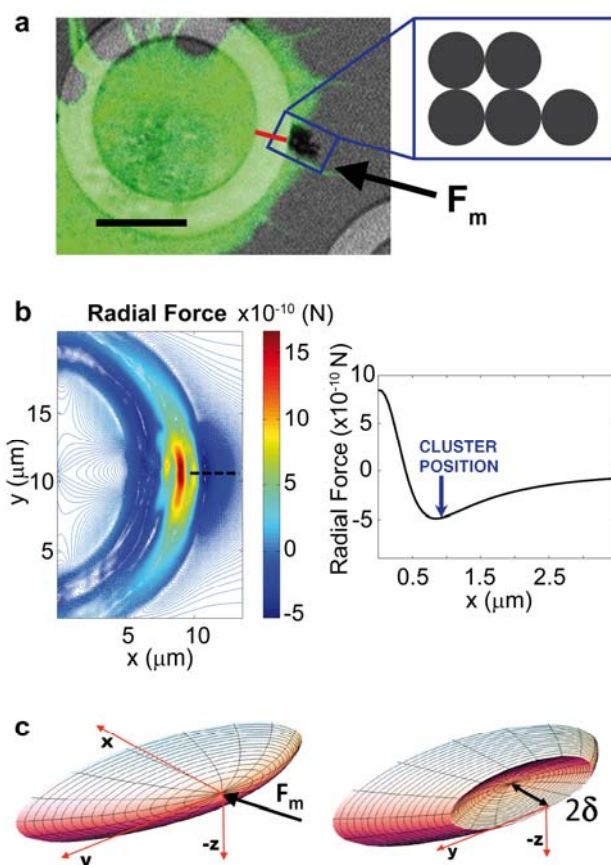
Quantification of the magnetic forces

The magnetic force producing such a deformation has been calculated according to the method described above. In the particular case of our experiment, F_m is due to a cluster of five particles as illustrated in Figure 4a. The cluster geometry, shape and orientation are carefully extracted from the confocal optical images, as illustrated in the zoom of Figure 4a. The map of the radial in-plane component (F_r) of the force exerted on the whole cluster is displayed in Figure 4b. Only the radial component is shown because the force causing the membrane deformation is perpendicular to the ring tangent in our experiment. The force is reported as a function of the position of the centre of the bottom-left bead in the cluster, which is translated all over the x-y plane. In Figure 4b the radial force on the cluster along the direction identified by the black dashed line in the left panel of Figure 4b is also plotted. For the beads configuration illustrated in Figure 4a, the simulated applied magnetic force is 480±50 pN. The main source of the error is uncertainty in the evaluation of the relative position between cluster and DW. In particular, the relative orientation of the external field with respect to the chip and therefore the position of the nucleated DW is set with an error of ±3 degrees, while the

spatial position of the beads in the cluster is estimated with an accuracy of 200 nm in the x,y plane.

Elastic membrane model of lateral indentation

To check the consistency between the mechanical stimulus applied to the cells and the deformation observed during the experiments, an elastic model of the cellular membrane has been used. Since the observed overall membrane deformation is small compared to the cell diameter, the external forces are mainly counterbalanced by the bending of the cell membrane, which is considered as an elastic shell[51] with Young modulus[52] $E= 5\cdot10^{-5}$ N/μm^2 and Poisson ratio[53] $v= 0.5$. The membrane is locally modeled as an elliptic

Figure 4: **a** Optical image showing the HeLa cell membrane deformed by a cluster of 5 magnetic beads. The sketch in the zoom represents the cluster geometry used for the evaluation of the magnetic force. Scale bar. 10 μm. **b** Left: contour plot of the simulated radial magnetic force, with respect to the ring, exerted on the bead cluster 100 nm above the nanostructure as function of the position of the left-bottom bead in the cluster. Right: plot of the radial force, evaluated along the black dashed line direction. The arrow represents the centre of the left-bottom bead in the cluster. **c** Sketch of the analytical surface used to model the cell membrane geometry, in proximity to the position where the mechanical load is applied, producing an indentation of 2δ.

surface (see Figure 4c) with positive Gaussian curvature everywhere. Considering the beads as a distributed load acting on the membrane, the elastic force that counterbalances the magnetic

one is expressed (see Supplementary Information for details) by the following equation[54,55]:

$$F_{el} = \frac{3c\pi E}{12^{3/4} \cdot (1-\nu^2)} h^{5/2} \frac{(2\delta)}{2(2-\beta)} \left(\frac{1}{R_y} + \frac{1}{R_z} \right) \qquad (4)$$

The (y,z) plane is tangent to the cell membrane at the point representing the geometrical centre of the area where the force is applied. The surface is locally characterized by the principal curvature radii *Ry* and *Rz*, whilst *2δ* is the indentation length produced by beads on the cell. It can be shown that the deformed shape of the cell membrane can be obtained reversing the shape of the paraboloid with respect to the plane at *x= δ*, producing a mirror-buckling.

The dimensionless parameter *c*= 1.15 is a constant obtained by minimizing a certain displacement functional under a nonholonomic constraint[56] and β indicates the portion of the free boundaries where the force is applied. The local curvature radii, extrapolated by the confocal images before the application of the mechanical stimulus, are R_y= 8±0.5 μm and R_z= 1.85±0.5 μm for the same cell displayed in Figure 3. The uncertainty depends on the microscope resolution and on the peculiar membrane profile smoothing required to average out the small HeLa protrusions. The cluster of beads produces a mechanical distributed load on an area of 2 μm^2 and the maximum lateral indentation is 2δ= 2.1 μm, as previously measured.

With these numbers, the calculated mechanical stimulus applied to the cell membrane is 575±134 pN, as calculated from Equation 4. The error arises from the uncertainty in the evaluation of the cell geometry (R_y, R_z, 2δ) from the optical images and in the actual parameters used in numerical calculations.

Noteworthy, this result is in excellent agreement with the magnetic force calculated through micromagnetic simulations (480±50 pN), thus confirming the reliability of the force quantification via magnetic simulations.

Potential of the DWT approach

The experimental data and the numerical models developed in this work, clearly demonstrate the capability of our technology to apply tuneable and localized forces on living cell, exerting lateral stimuli affecting the cell membrane shape. Magnetic structures patterned on-chip are exploited to implement a non-invasive manipulation method, fully biocompatible and integrated with conventional setups for advanced cell investigation. No relevant limitations on the numerical aperture, working depth, magnification or imaging modality have emerged so far. In this paper we used a upright confocal microscope, but also an inverted microscope can be employed if magnetic structures are fabricated on transparent substrates. With respect to previous works[41,45], the geometry of the magnetic rings has been optimized to maximize the magnetic force. This leads to values of *Fm*, approaching the nN range over a few μm^2 area, which are suitable for mechanobiology studies where concentrated forces on specific areas of the cell are required[23].

Moreover, by applying different external magnetic fields, a fine tuning of the applied forces can be reached[49].

Furthermore, with this approach, a precise quantification of the applied forces can be performed via micromagnetic simulations, using as input parameters only the actual bead position with respect to the DW in the conduit. In perspective, the system can be integrated with a dedicated software which calculates the mechanical stimuli strength in real time, thus providing biologists with a quantitative tool for the application of localized forces to cells.

Conclusions

An on-chip platform based on magnetic domain wall tweezers, allowing for the application of finely controlled and localized forces on target living cells, is presented.

It is demonstrated that this technology is suitable for the manipulation of 1 μm superparamagnetic beads in order to bring them in contact to the HeLa cells membrane, where particles can exert a magnetic force in the order of hundreds pN. Such mechanical stimulus produces a local deformation of the cellular membrane, which is precisely quantified via experiments and simulations.

This magnetic technology is a unique example of an integrated and fully biocompatible tool suitable for *in vitro* mechanobiology studies, requiring the application of localized mechanical stimuli. Noteworthy, the manipulation is actuated via quasi-static and non-invasive magnetic fields, generated via small permanent magnets underneath the chip and microscope stage. This allows for an easy integration of the system in confocal microscopy systems suitable for sophisticated real time investigation of the cell functionalities in response to applied mechanical stimuli.

Acknowledgments

References

1   P. Skehan, R. Storeng, D. Scudiero, A. Monks, J. McMahon, D. Vistica, J. Warren, H. Bokesch, S. Kenney and M. Boyd, *Natl Cancer Inst* 1990, **82**, (13): 1107-1112.
2   P. Dittrich, A. Manz, *Nature Reviews Drug Discovery*, 2006, **5**, 210-218.
3   J. Kim, I. Hwang, D. Britain, T. Chung, Y. Sun and D. Kim, *Lab Chip*, 2011, **11**, 3941.

ARTICLE

4   J. Quan, I. Saaem, N. Tang, S. Ma, N. Negre, H. Gong, K. White and J. Tian, *Nature Biotechnology*, 2011, **29**, 449–452.
5   N. Wang, J. Butler, D. Ingber *Science*, 1993, **260**, 1124-1127.
6   J. Dobson, *Nat. Nanotechnol.,* 2008, **3**, 139.
7   T. Xu, W. Yue, C. Li, X. Yaod and M. Yang, *Lab Chip*, 2013, **13**, 1060-1069.
8   M. Ferrari, *Nature Rev. Cancer,* 2005, **5**, 161–171.
9   D. Peer, J. Karp, S. Hong, O. Farokhzad, R. Margalit and R. Langer, *Nature Nanotechnology*, 2007, **2**, 751 - 760.
10   V. Vogel and M. Sheetz, *Nat. Rev. Mol. Cell Biol.* 2006, **7**, 265.
11   M. Köpf, *Phys. Rev. E* 2015, **91**, 012712
12   Q. Wang, X. Zhang, Y. Zhao, *J Micromec Microeng*, 2013, **23**, (1):015002.
13   Y. Li, H. Liu, Y. Huang, L. Pu, X. Zhang, C. Jiang and Z. Jiang, *Int J Mol Med.,* 2013, **31**, 1234-42.
14   J. Wang, Y. Zhang, N. Zhang, C. Wang, T. Herrler and Q. Li, *Cell. Mol. Life Sci.*, 2015, **72**, 2091–2106.
15   Y. Wang, W. Wang, Z. Li, S. Hao and B. Wang, *Biomech Model Mechanobiol*, 2015, **4**, 0743.
16   D. Kim, P. Wong, J. Park, A. Levchenko, and Y. Sun*, Annu. Rev. Biomed. Eng*., 2009, **11**, 203.
17   J. Rajagopalan and M. Saif, *J. Micromech. Microeng*., 2011, **21**, 54002.
18   A. LaCroix, K. Rothenberg, B. Hoffman, *Annual Review of Biomedical Engineering*, 2015, **17**, 287-316.
19   Y. Shao and J. Fu , *Adv. Mater.,* 2014, **26**, 1494 .
20   W. Polacheck, R. Li, S. Uzel and R. Kamm, *Lab Chip*, 2013, **13**, 2252-2267.
21   Y. Cui, F. Hameed, B. Yang, K. Lee, C. Pan, S. Park and M. Sheetz, *Nature Communications,* 2015, **6**, 6333.
22   K. Wong, J. Chan, R. Kamm and J. Tien, *Annu. Rev. Biomed. Eng.* 2012, **14**, 205.
23   A. Kumar, M. Mazzanti, M. Mistrik, M. Kosar, G. Beznoussenko, A. Mironov, M. Garre`, D. Parazzoli. G. Shivashankar, G. Scita, J. Bartek, and M. Foiani, *Cell*, 2014, **158**, 633-646.
24   T. Puntheeranurak, I. Neundlinger, R. Kinne and P. Hinterdorfer, *Nature Protocols*, 2011, **6**,1443–1452.
25   M. Rodriguez, P. McGarry and N. Sniadecki, *Appl. Mech. Rev*, 2013, **65**, 6.
26   M. Monticelli, A. Torti, M. Cantoni, D. Petti, E. Albisetti, A. Manzin, E. Guerriero, R. Sordan, G. Gervasoni, M. Carminati, G. Ferrari, M. Sampietro and R. Bertacco, doi10.1002/smll.201500916.
27   A. Ashkin and J. Dziedzic, *Science,* 1987, **235**, (4795) 1517–1520.
28   A. Ashkin, J. Dziedzic, and T. Yamane, *Nature,* 1987, **330**, 769–771.
29   H. Zhang, k. Liu, *J. R. Soc. Interface*, 2008, **5**, 671–690.
30   S. Ayano, Y. Wakamoto, S. Yamashita and K. Yasuda, *Biochem. Biophys. Res. Commun*, 2006, **350**, 678–684.
31   M. Rasmussen, L. Oddershede, H. Siegumfeldt, *Appl Environ Microbiol*, 2008, **74**, 8.
32   L. Kremser D. Blaas, and E. Kenndler, *Electrophoresis*, 2004, **25**, 2282–2291.
33   C. Cabrera, P. Yager, *Electrophoresis*, 2001, **22**, 355–362.
34   M. Hughes, *Electrophoresis*, 2002, **23**, 2569–2582.
35   C. Courtney, C. Demore, H. Wu, A. Grinenko, P. Wilcox, S. Cochran and B. Drinkwater, *Applied Physics Letters*, 2014, **104**, 154103.
36   T. Deng, G. Whitesides, M. Radhakrishnan, G. Zabow, M. Prentiss, *Appl. Phys. Lett.,* 2001, **78**, 1775.
37   A. De Vries, B. Krenny, R. van Driel, J. Kanger, *Biophys. J.,* 2005, **88**, 2137.
38   B. Yellen, G. Friedman, *Adv. Mater.,* 2004, **16**, 111.
39   H. Ebrahimian, M. Giesguth, K.-J. Dietz, G. Reiss and S. Herth, *Appl. Phys. Lett*., 2014, **104**, 063701.
40   K. Gunnarsson, P. Roy, S. Felton, J. Pihl, P. Svedlindh and H. Berner, S. Oscarsson, *Adv. Mater,* 2005, **17**, 1730.
41   M. Donolato, P. Vavassori, M. Gobbi, M. Deryabina, M. Hansen, V. Metlushko, B. Ilic, M. Cantoni, D. Petti, S. Brivio, R. Bertacco, *Adv. Mater.,* 2010, **22**, 2706.
42   R. Bertacco, M. Donolato, M. Gobbi, M. Cantoni, S. Brivio, D. Petti, P. Vavassori, PCT/EP2010/000879 (2010), nanoGune Consolider.
43   A. Torti, V. Mondiali, A. Cattoni, M. Donolato, E. Albisetti, A. Gosnet, P. Vavassori and R. Bertacco, *Appl. Phys. Lett.*, 2012, **101**, 142405.
44   M. Leal, A. Torti, A. Riedinger, R. La Fleur, D. Petti, R. Cingolani, R. Bertacco, and T. Pellegrino, *ACS Nano*, 2012, **6**, 10535-10545.
45   M. Donolato, A. Torti, E. Sogne, N. Kostesha, M. Deryabina, P. Vavassori, M. Hansen, R. Bertacco, *Lab Chip,* 2011, **11**, 2976.
46   J. Riedl, A. Crevenna, K. Kessenbrock, J. Yu, D. Neukirchen, M. Bista, F. Bradke, D. Jenne, T. Holak, Z. Werb, M. Sixt and R. Wedlich-Soldner, *Nat Methods*, 2008, **5,** 605.
47   D. Donahue, *1999 OOMMF User's Guide*, Version 1.0. Interagency Report NISTIR, 2004, **6376**, 3.
48   L. Landau, E. Lifshitz, *Pergamon Press*, 1960.
49   M. Monticelli, E. Albisetti, D. Petti, D. Conca, M. Falcone, P. Sharma and R. Bertacco, J. Appl. Phys., *2015,* **117**, 17B317.
50   O. Bondar, D. Saifullina, I. Shakhmaeva, I. Mavlyutova and T. Abdullin, *Acta Naturae*, 2012, **4**, 78–81.
51   A. Vaziri and L. Mahadevan, *Proceedings of the National Academy of Sciences*, 2008, **105**, (23)7913-7918.
52   K. Kim, C. Cho, E. Park, M. Jung, K. Yoon and H. Park, *PloS one*, 2012, **7**, 30066.
53   T. Jadidi, H. Seyyed-Allaei, M. Tabar and A. Mashaghi, *Frontiers in bioengineering and biotechnology*, 2014, **2**.
54   D. Vella, A. Ajdari, A. Vaziri A. Boudaoud, *Physical review letters*, 2012, **109**, 144302.
55   E. Ventsel and T. Krauthammer, *CRC press*, 2001.
56   A. Pogorelov, *American Mathematical Soc*., 1988, **72**.